

DEVELOPMENT OF NOVEL TUNABLE DUAL-BAND NEGATIVE INDEX METAMATERIAL USING OPEN STUB-LOADED STEPPED-IMPEDANCE RESONATOR

A. R. H. Alhawari¹, A. Ismail^{1, 2, *}, M. A. Mahdi¹, and R. S. A. Raja Abdullah¹

¹Centre of Excellence for Wireless and Photonics Network, Department of Computer and Communication Systems Engineering, Faculty of Engineering, Universiti Putra Malaysia, 43400 UPM Serdang, Selangor, Malaysia

²Institute of Advanced Technology, Universiti Putra Malaysia, Malaysia

Abstract—This study reports on tunable planar metamaterial design that is capable to achieve dual-band negative index of refraction responses operating in microwave regime. Its distinctive characteristic is the usage of tuning open stub-loaded stepped-impedance resonators. Parameters retrieval algorithm, and full-wave simulation of prism-shaped structure were carried out to validate the negative refraction characteristics of metamaterial structure. The results predict its prospect as a very promising alternative to the conventional ones, which is compatibly applicable on various potential microwave devices especially when dual-band function is required. In addition to that, its design flexibility offers a various frequency bands at any possible choice, which is alterable together with any design parameters changes.

1. INTRODUCTION

In the year 1968, physicist Veselago in his early seminal work [1] theorized a new type of material that can exhibit negative electrical permittivity (ϵ) and negative magnetic permeability (μ) simultaneously across a common frequency band. He theoretically created a lossless metamaterial (MTM) that exhibits negative ϵ and μ ; shows atypical properties, which is not found in nature, and is capable to focus the electromagnetic radiation. Later, Pendry and his

Received 22 August 2011, Accepted 11 October 2011, Scheduled 15 October 2011

* Corresponding author: Alyani Ismail (alyani@eng.upm.edu.my).

co-workers presented the first metamaterial [2] and [3]. They showed that in such material, the existence of negative ε and μ can be exhibited using conductive wires and split-ring resonators (SRRs) respectively. Afterwards, Smith et al. (2000) [4] and Shelby et al. (2001) [5] validated this idea. They experimentally demonstrated the first metamaterial that shows simultaneously negative ε and μ by constructing two-dimensional periodic structure unit cells of SRRs with copper strips that verifies its extraordinary properties at microwave frequencies.

Since the success of metamaterial design mostly depends on the shape and the geometry of the unit cell, numerous novel methods have been proposed to investigate the potential applications [6–21]. The majority of the aforementioned metamaterial studies focused on achieving the desired electromagnetic response at a single frequency band. In order to achieve a dual band negative index, a typical method is to construct the composite with the ability of producing magnetic responses at two frequency bands [22–24]. It will then be combined with material that allows negative permittivity at the corresponding frequency bands.

Recently, several types of artificial metamaterial have been reported to achieve dual-band negative index response [25–28]. A metamaterial structure having magnetic resonances at two different frequencies providing effective negative permeability values over two separate bandwidths is proposed in [25]. The metamaterial unit cell topology is made of a single loop of conductive strip printed over a dielectric substrate with a special winding geometry. Another dual-band negative refractive metamaterial is reported in [26] using cut wire pairs and continuous wires. In this design, the cut wire pairs structure can exhibit negative permeability over two frequency bands by modifying the length or width of the cut wire. While design [27], used cut wire pairs and continuous wire elements to produce dual-frequency double-negative response composite metamaterial, where the dual-frequency operation is obtained by employing cut wire pairs of two different lengths within the unit cell. Other metamaterial designs that exhibit double negative over two frequency bands are reported in [28]. These metamaterials consist of electric resonant parallel strips with one or two magnetic resonant spirals. However, these reported designs bring along discoveries of some related problems, primarily, the materials are found simply untunable, apart from generally producing quite narrow bandwidths, which consequently limit the range of potential applications, notwithstanding of the fabrication and utilization complexity. The setbacks necessitate endeavors to overcome the range limitation of applications prioritizing simplification of design and usage. Therefore, more investigation on the electromagnetic

response of the dual structure in details should be done to further assist design considerations in order to improve their utilization in multi-band applications.

In this paper, we introduce a novel resonator named as an “open stub-loaded stepped-impedance resonator” (open stub-loaded SIR) to design metamaterial that exhibit dual-band negative refractive index over different frequency bands. The metamaterial unit cell in the design is constructed using single open stub-loaded SIR, which is printed on both sides, on top and bottom of the dielectric substrate. The parameters efficiency of the proposed metamaterial unit cell was meticulously selected from numerous simulations based on the characteristics of reflection and transmission coefficient results. The design properties are further analyzed theoretically before being re-confirmed by simulation to verify that it was soundly designed. Accordingly is manufacturable for potential diverse applications of microwave frequency band with its advantages of simple tunability at remarkable loss reduction whilst is also adjustable for low and high frequency regimes.

The paper is organized as follows: Section two presents the basic structure of half-wavelength stepped-impedance resonator and its main characteristics. It is followed by Section three, which presents the proposed open stub-loaded SIR and provides a critical analysis on it. Section four is comprised of three subsections: 1. Open stub-loaded SIR design. 2. Description of the proposed MTMs structures. 3. Coupling structure. Then along comes Section five on analyses and simulations of the MTM design. Prism-shaped structure validation follows in Section six. Finally, Section seven concludes the letter including its significance and practical applications suitable for the obtained results.

2. CHARACTERISTICS OF BASIC STRUCTURE OF HALF-WAVELENGTH STEPPED-IMPEDANCE RESONATOR

Microstrip stepped-impedance resonators (SIRs) have been extensively used in microstrip microwave devices design due to its size reducibility and harmonic control. Moreover, it has been shown that the SIR is wide-range tunable based on the length ratio of low-impedance section over high-impedance section [29–34]. Typically, the structure of half-wavelength ($\lambda_g/2$) microstrip SIR consists of two transmission lines with different characteristic impedance; high-impedance section (Z_1) and low-impedance section (Z_2); and electrical lengths of θ_1 and θ_2 as shown in Fig. 1 [35]. The most important electrical parameter in

characterizing the properties of SIR is called impedance ratio (R_Z), and it can be defined as [35]:

$$R_Z = Z_2/Z_1 \tag{1}$$

In order to investigate the fundamental and higher order resonance frequencies conditions of SIR shown in Fig. 1, regardless of the step discontinuities effects in the transmission line and the fringing fields at the open end, the input impedance (Z_{in}) can be expressed as follows [35]:

$$Z_{in} = jZ_2 \left(\frac{Z_1 \tan \theta_1 + Z_2 \tan \theta_2}{Z_2 - Z_1 \tan \theta_1 \tan \theta_2} \right) \tag{2}$$

The fundamental resonant frequency (f_0) which is corresponding to the electrical length θ_0 occurs when $Z_{in} \rightarrow \infty$ ($Y_{in} = 0$) as follows [35]:

$$Z_2 - Z_1 \tan(\theta_1) \tan(\theta_2) = 0, \tag{3}$$

then,

$$\tan(\theta_1) \tan(\theta_2) = Z_2/Z_1 = R_Z \tag{4}$$

For practical application, we assume that $\theta_1 = \theta_2 = \theta_0$, thus

$$\theta_0 = \tan^{-1} \left(\sqrt{R_Z} \right) \tag{5}$$

The first spurious frequency (f_{s1}) which is corresponding to the electrical length θ_{s1} occurs at [35]:

$$\tan(\theta_{s1}) = \infty \tag{6}$$

Accordingly, from Equations (5) and (6), f_{s1} can be obtained as follows [35]:

$$\frac{f_{s1}}{f_0} = \frac{\theta_{s1}}{\theta_0} = \frac{\pi}{\left(2 \tan^{-1} \left(\sqrt{R_Z} \right) \right)} \tag{7}$$

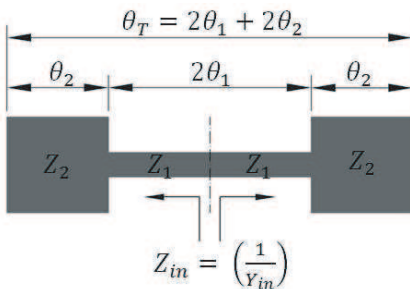


Figure 1. Conventional Schematic of a half-wavelength stepped-impedance resonator.

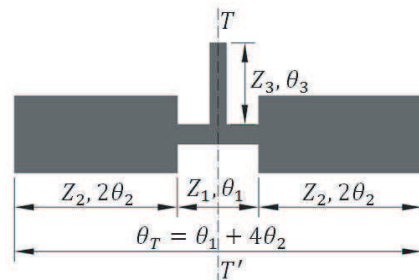


Figure 2. Structure of the proposed open stub-loaded SIR applied in the design.

It is clear from Equations (5) and (7) that the fundamental and the spurious frequencies can be controlled by the impedance ratio R_Z . The smaller the value of R_Z , the further the spurious frequencies will be from the fundamental frequency. Whenever this is applied, it is found that the resonator length is optimally minimized. This is beneficial to fit miniaturization demand in the industry.

3. ANALYSIS ON THE PROPOSED OPEN STUB-LOADED STEPPED-IMPEDANCE RESONATOR

The proposed open stub-loaded SIR consists of a modified microstrip half-wavelength resonator and a open stub-loaded as illustrated in Fig. 2, where Z_3 and θ_3 represent the characteristic impedance and the electrical length of the open stub-loaded, respectively. Compared to the short-circuited stub-loaded resonator reported in [36–38], the open stub-loaded resonator is less complicated to fabricate when it comes to printing a circuit layout.

The illustration in Fig. 2 shows that the open stub-loaded SIR is symmetrical to the T - T' plane, yet, the resonator is analyzable using odd-mode and even-mode method [39–42]. The odd-mode and even-mode resonances can be separately extracted by enforcing the input impedance (Z_{in}) to zero [39]. In order to simplify the analysis, we assumed that $Z_1 = Z_3$ thus, the resonances occur under the conditions given below [40–42]:

- For odd-mode resonance condition (Fig. 3(a)):

$$2 \tan \left(\frac{\theta_1}{2} \right) \cdot \tan (2\theta_2) = R_Z \tag{8}$$

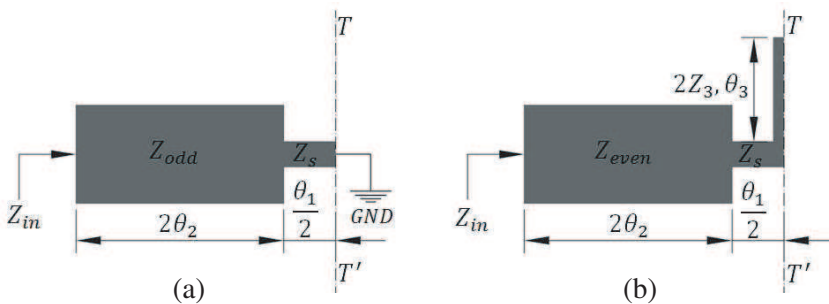


Figure 3. Approximate transmission line circuit model of the open stub-loaded SIR in Fig. 2: (a) odd-mode equivalent circuit, and (b) even-mode equivalent circuit.

- For even-mode resonance condition (Fig. 3(b)):

$$2 \cot \left(\frac{\theta_1}{2} + \theta_3 \right) = -R_Z \cot (2\theta_2) \quad (9)$$

Applying the previously defined Equations (9) and (10) in a suggested assumption, given $\theta_1 = \theta_2 = \theta$, at the length ratio (α) of the proposed open stub-loaded SIR is then defined as:

$$\alpha = \left(\frac{\theta_3}{\theta} \right) \quad (10)$$

Therefore, odd-mode and even-mode resonance conditions can be derived as the following equations after substituting (11) into (9) and (10):

$$2 \tan \left(\frac{\theta}{2} \right) \cdot \tan (2\theta) = R_Z \quad (\text{odd-mode}) \quad (11)$$

$$2 \cot \left(\left(\frac{1}{2} + \alpha \right) \theta \right) = -R_Z \cot (2\theta) \quad (\text{even-mode}) \quad (12)$$

Thus, from Equations (12) and (13) f_2/f_1 can be expressed as:

$$\frac{f_2}{f_1} = \frac{\theta_{\text{even-mode}}}{\theta_{\text{odd-mode}}} = \frac{\pi}{(2.5 + \alpha) \cdot \cos^{-1} \left(\frac{-2 - \sqrt{4 + 4R_Z + 2R_Z^2}}{-(4 + 2R_Z)} \right)} \quad (13)$$

According to the previously obtained equations that we derived (12)–(14), it can be observed that the fundamental frequency and the first higher-order frequency occur in the odd-mode and even-mode, respectively. Furthermore, the open stub-loaded (Z_3, θ_3) impinge on the even-mode resonant frequencies only, without affecting the odd-mode resonant frequencies. Therefore, the open stub-loaded SIR is easily controlling the resonant frequencies and yet still capable to achieve the design of negative refraction index metamaterial with two different frequency bands. Here, the first band which is associated with the first odd resonance can be adjusted by properly choosing a suitable combination of characteristic impedances (Z_1 and Z_2) and the electrical length (θ_1 and θ_2) of SIR. The central frequency of the second band that corresponds to the first even resonance is easily tuned by adjusting the dimensions of the open stub-loaded (Z_3, θ_3) while the characteristic of the first resonant frequency remains.

In order to verify the above results, the open stub-loaded SIR in Fig. 2 was simulated using a full-wave electromagnetic simulation (CST Microwave Studio) [43]. In this case, two microstrip lines with 50 ohm characteristic impedance are used to feed the proposed open

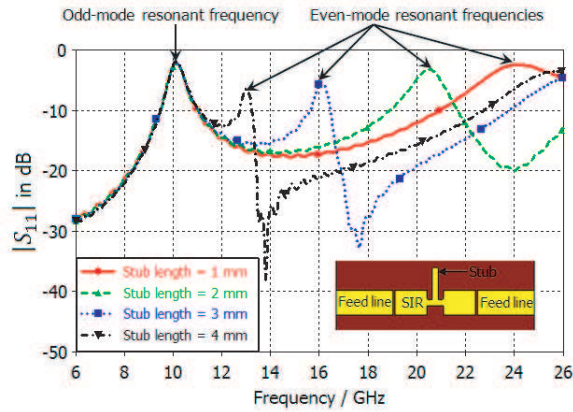


Figure 4. Simulated operating frequencies characteristics against stub length, on a substrate thickness of 0.787 mm with a relative dielectric constant of 2.2 ($Z_1 = Z_3 = 105.78 \Omega$, $Z_2 = 51.03 \Omega$, $\theta_1 = \theta_2 = 24.2^\circ$ at center frequency of 10 GHz).

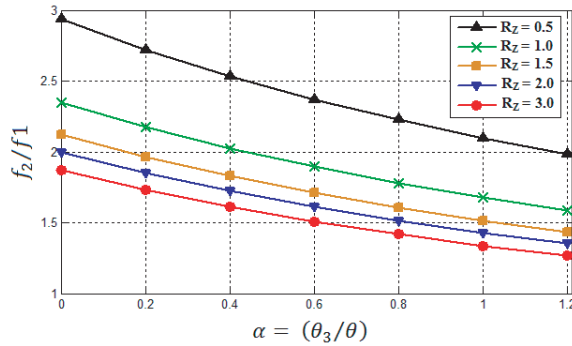


Figure 5. Normalized ratios of the second resonant frequency to the fundamental frequency of the proposed open open stub-loaded SIR under different values of R_Z and α .

stub-loaded SIR under weak coupling. Fig. 4 demonstrates that any increment of the open stub-loaded length will affect the first even-mode resonance frequency and shift it down within a wide range and vice versa, while the fundamental odd-mode resonant frequency remains the same.

Figure 5 shows the relationship between the length ratio (α) and normalized ratio of the second resonant frequency with respect to the fundamental frequency (f_2/f_1) taking R_Z as a parameter. As seen in

Fig. 5, the first two resonant frequencies f_2 and f_1 can be determined by scrupulously choosing optimal values of two main parameters α and R_Z . The realizable f_2/f_1 is found to be between 1.26 and 2.94. This value of f_2/f_1 is similar with those obtained in [42]. Theoretically, wider range of f_2/f_1 is obtainable by changing R_Z . In comparison to the conventional SIR reported in [40] and [41], the realizable f_2/f_1 range of the proposed open stub-loaded SIR presented in this paper is wider even with the same values range of R_Z .

4. THE PROPOSED OPEN STUB-LOADED SIR METAMATERIAL DESIGN AND ITS PROPERTIES

4.1. Open Stub-loaded SIR Design

The open stub-loaded SIR was designed at a center frequency of 10 GHz, where the total electric length $\theta_T = 5\theta$. The initial circuit dimensions were calculated as follows: $R_Z = 0.482$, $Z_1 = Z_3 = 105.78 \Omega$, $Z_2 = 51.03 \Omega$, $\theta_1 = \theta_2 = 24.2^\circ$ and $\theta_3 = 19.9^\circ$. Then, these parameters were optimized by CST Microwave Studio simulator [43]. After a few repetitions in the optimization process, the structural parameters of every open stub-loaded SIR shown in Fig. 6 are summarized in Table 1.

Table 1. Design parameters of every open stub-loaded SIR.

Parameter	$l_1 = l_3$	l_2	l_{stub}	W_1	W_2	W_{stub}
Dimension (mm)	3.1	1.5	1.25	2.35	0.6	0.5

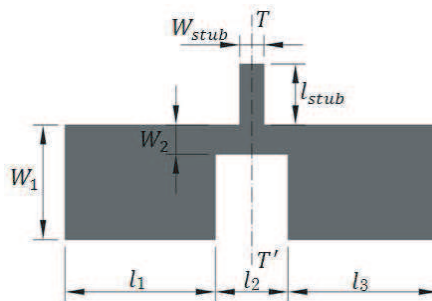


Figure 6. Open stub-loaded SIR design parameters.

4.2. Description of the Proposed MTM Structure

The aim of this study is mainly to design planar structure that can exhibit dual-band negative index of refraction operating in microwave frequency regime, and investigate its properties. Fig. 6 shows the model of the proposed MTM structure used in the applied designs. The MTM structure where each unit cell is mainly composed of open stub-loaded SIR to simplify production of MTMs as the first design is presented in the previous section. The MTM is designed to have etched open stub-loaded SIRs arranged on the opposite sides i.e., on top and bottom; of the dielectric substrate as illustrated in Fig. 7(a). This MTM design technique offer simplified structures, advantage of compactness, capability to produce bands of negative refraction index at microwave frequency and easier fabrication in planar technology for instance microstrip. It generally comprises periodic elements, and gains its properties from the structure as a whole rather than directly from the constitutive properties of a single component.

4.3. Coupling Structure

The coupling coefficient between two adjacent microstrip open stub-loaded SIRs (either on the top or bottom surface of the substrate) can be extracted using three-dimensional electromagnetic simulator [43]. In this case, both resonators should be weakly coupled to their feeds in order to avoid coupling loading effect from the first and second feeds

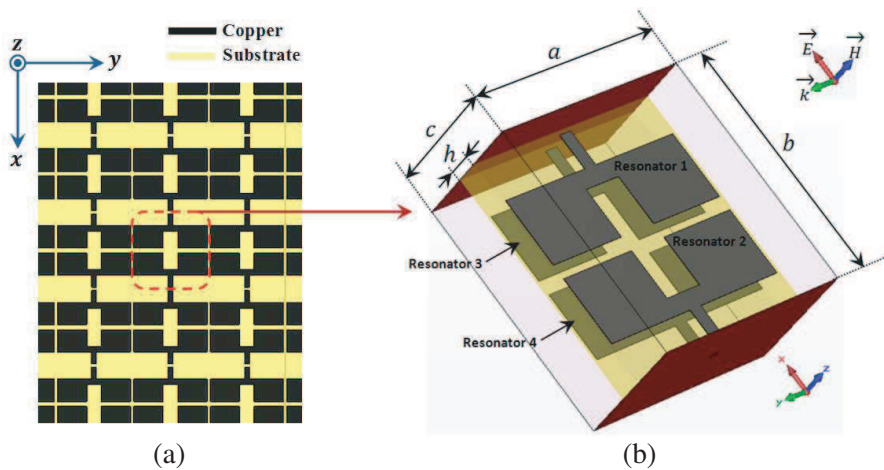


Figure 7. (a) MTM structure and (b) perspective view for its unit cell.

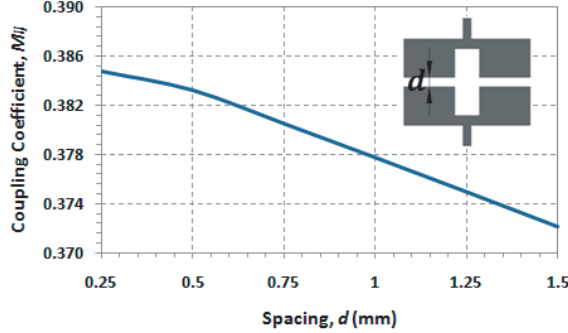


Figure 8. Coupling coefficient between resonators versus the distance, d (substrate thickness, $h = 0.787$ mm and dielectric constant, $\epsilon_r = 2.2$) for the proposed MTM.

Reason-wise is to determine the appropriate gaps between the adjacent resonators in the design. The general formulation for extracting the coupling coefficients of two adjacent resonators is given in equation below [44]:

$$M_{ij} = \pm \left(\frac{f_2^2 - f_1^2}{f_2^2 + f_1^2} \right) \quad (14)$$

where f_1 and f_2 are the odd-mode and even-mode resonant frequencies respectively and M_{ij} is the coupling coefficient between i th and j th resonator.

Figure 8 plots the value of coupling coefficients M_{ij} against the coupling spacing (d) between two adjacent resonators; simulation deduced that when d increases M_{ij} decreases. The value of d for all the mentioned MTM designs is constant at 0.5 mm.

5. ANALYSIS AND SIMULATION

The proposed MTM unit cell with dimensions of $a = b = 8$ mm and $c = 6$ mm is designed on Rogers RT/Duroid 5880 substrate with dielectric constant $\epsilon_r = 2.2$, loss tangent $\delta = 0.0009$, and thickness $h = 0.787$ mm using full-wave electromagnetic simulator [42] to obtain the S -parameters in terms of return loss (S_{11}) and insertion loss (S_{21}) magnitudes. For numerical simulation purposes, we put the configuration of MTM in a two-port waveguide and excited with an electric field along the x -direction and a magnetic field perpendicular to the conducting elements plane along the z -direction.

In order to verify the electromagnetic properties of the designed MTM, the retrieval algorithm described in [45–47] was used to

obtain the effective constitutive parameters based on the reflection and transmission coefficient characteristics. The effective constitutive parameters are: the impedance (z), the relative effective permittivity (ϵ), the permeability (μ), and the refractive index (n) are obtainable by:

$$z = \pm \sqrt{\frac{(1 + S_{11})^2 - S_{21}^2}{(1 - S_{11})^2 - S_{21}^2}} \quad (15)$$

$$e^{(jnk_0d)} = X \pm j\sqrt{(1 - X^2)} \quad (16)$$

$$X = \frac{(1 - S_{11}^2 + S_{21}^2)}{(2S_{21})} \quad (17)$$

$$\epsilon = n/z \quad (18)$$

$$\mu = n \times z \quad (19)$$

where k_0 is the wave-number of the incident wave in free space and d indicates the slab thickness of the MTM.

Figure 9 shows the simulated S -parameters characteristics of MTM structure. We can observe from Fig. 9 that there are two transmission peaks occur at 5.94 GHz and 22.63 GHz respectively. The first transmission passband indicates region of the first magnetic resonance which is mainly depends on the coupling between the resonators. While the second transmission passband indicates the second magnetic resonance occurs at the center frequency of the first even resonance in the open stub-loaded SIR. This MTM structure also has electric resonance region occurs at 9 GHz produced by open stub-loaded SIR, and its electric resonance frequency is often above the first magnetic resonance frequency. Moreover, the first transmission peak (5.94 GHz) indicates that the sample impedance z is closer to 1

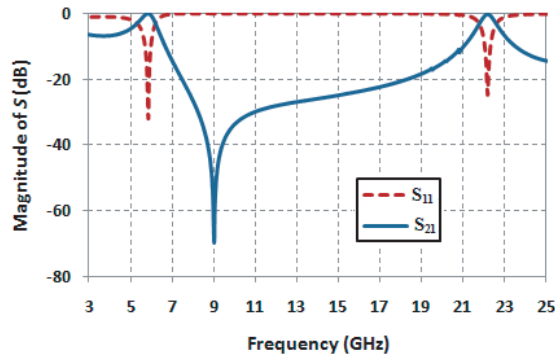


Figure 9. MTM S -parameters simulated results.

compared to the second transmission peak (22.63 GHz) with a little reflection. The mentioned results demonstrate the appearance of negative refractive index over two frequency bands which indicate the existence of dual-band negative index from this structure. This could be verified by retrieving the effective constitutive parameters as point to be discussed next.

From the simulated results given in Fig. 10, it is observed that the extracted real part of the permeability μ is simultaneously negative over two narrow frequency bands, which are 5.79–7.18 GHz and 21.6–22.68 GHz, respectively. The effective permittivity ϵ is negative over a very broad band from 5.5–21.04 GHz. From the real part of ϵ , it is noted that there is anti-resonance at the electric resonance region, and the imaginary part of ϵ is negative at the same frequency. In agreement with the two overlapping regions observed in the microwave frequency range where ϵ and μ are both negative, our sample structure in fact exhibits two left-handed passbands at 5.7–7.27 GHz and 8.9–22.68 GHz and, as shown in Fig. 10(d), the corresponding refractive index (n) values are negative in both regions. The wideband region of the negative index appeared in the second region, most probably due

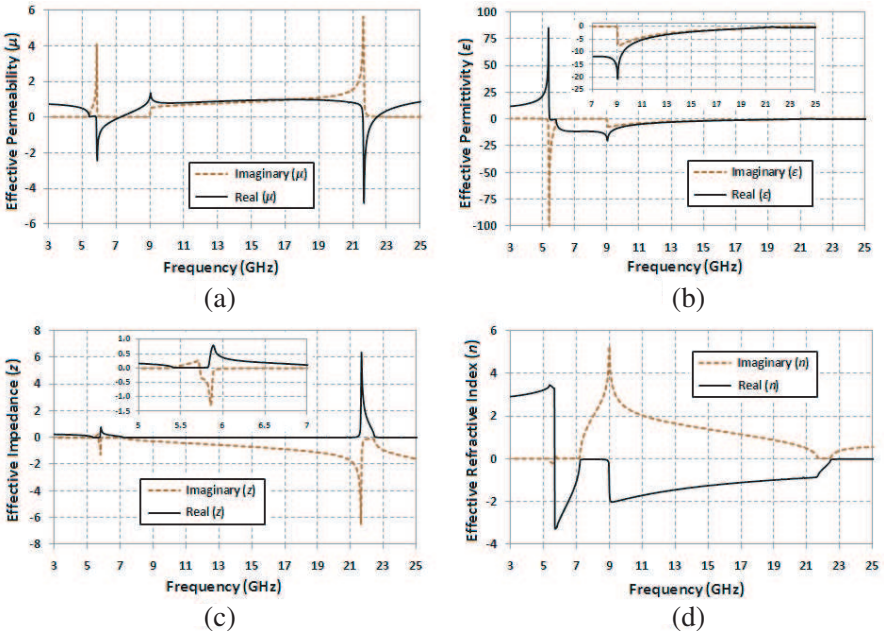
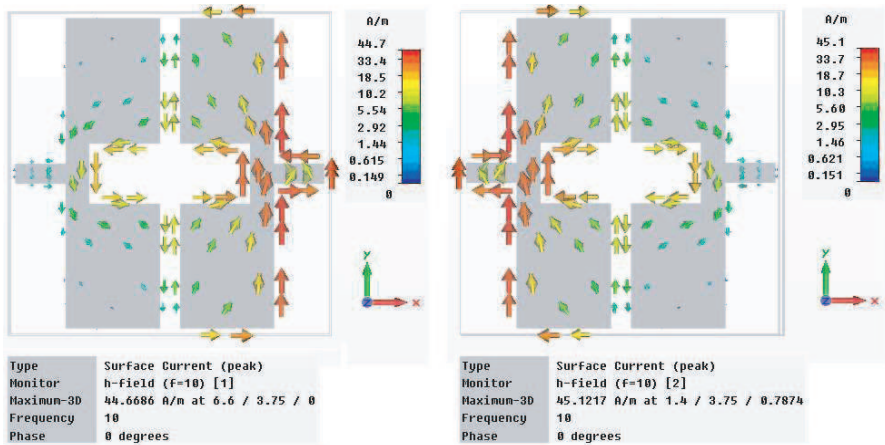
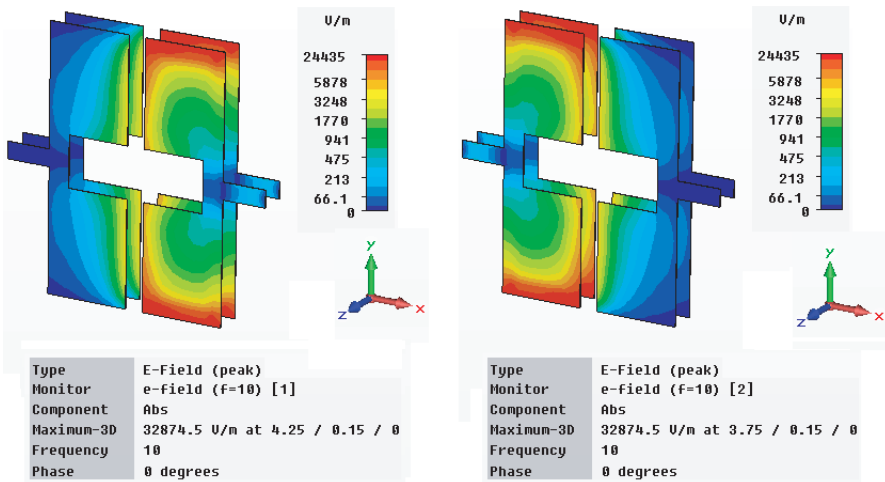


Figure 10. Retrieved effective parameters of the MTM: (a) permeability, (b) permittivity, (c) impedance and (d) refractive index.

to enhanced coupling among the resonators in the unit cell structure. The negative band region starts from the electric resonance peak and ends at the second magnetic resonance peak. This negative band of refraction is tunable via the open stub as mentioned in Section 3. These findings indicate that the effective parameters of the structure did produce negative refractive index over a broader wideband region than the region produced by the MTMs recently reported in [25–28].



(a)



(b)

Figure 11. (a) Surface current and (b) electric field distribution magnitude for at the frequency of 10 GHz.

Hence, it is exploitable in the design of microwave devices like antennas that may yield high quality performance with smaller sizes at lower cost. Moreover, these results clearly show that the proposed MTM can be alternatives to the ordinary MTM designs specifically those operated on a dual-band.

To further illustrate the nature of the MTM design, we analyzed the structure to understand its observed performance. Fig. 11 demonstrates the surface current and the magnitude of the electric field distributions on the conducting surface of MTM at the frequency where the negative index exists. Red color indicates strong positive values and blue color indicates strong negative values. As Fig. 11(a) depicts, the structure has circulating currents as described in details by the direction of arrows. In Fig. 11(b), the electric field is strong at the edges of the thin line gap due to the strong coupling; thus any change in dimensions of the gap will strongly affect the electric field distribution and subsequently the surface current will also change, which inevitably leads to behavioral changes of the structure.

6. PRISM-SHAPED STRUCTURE SIMULATION VALIDATION

One of the techniques to validate the negative refractive index behavior of the MTM obtained from retrieval algorithm is via refraction experiment prism simulation for microwave beam deflection observing purpose in [5, 48, 49]. Here we present full wave simulation for the proposed MTM prisms, which are designed similarly to the actual samples used in the experiments reported in [5]. The model of MTM prism is depicted in Fig. 12. The prism has an inclination angle, $\theta_i = 19^\circ$, where 10 unit cells are arranged along y -axis and 10 unit cells along z -axis. In the simulation, electromagnetic (EM) wave is guided by a rectangular waveguide and normally injected on the prism front face. Both waveguide and prism have perfect electric conductor (PEC) conditions on the top and bottom planes, conversely, other edges have perfect match layer (PML) conditions. In Fig. 13, the magnitude of the electric field distribution is illustrated at the frequency of 6 GHz, 7.1 GHz, 13 GHz, 15 GHz, 17.5 GHz, and 19.5 GHz, where the negative refractive index regions. The simulated results show that with incident angle of 19° , the negative refraction angle is -12° , -3° , -10° , -6° , -50° , and -60° respectively. Then based on Snell's law, its refractive indices are calculated as -0.64 , -0.16 , -0.53 , -0.32 , -2.35 , -2.66 respectively. Congruously the calculated negative refractive index from the refraction angle is in good agreement with the one obtained from the retrieval result.

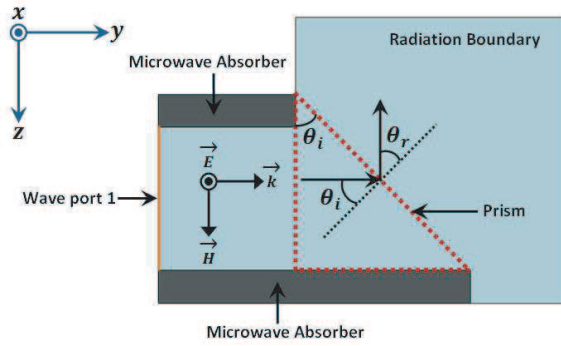
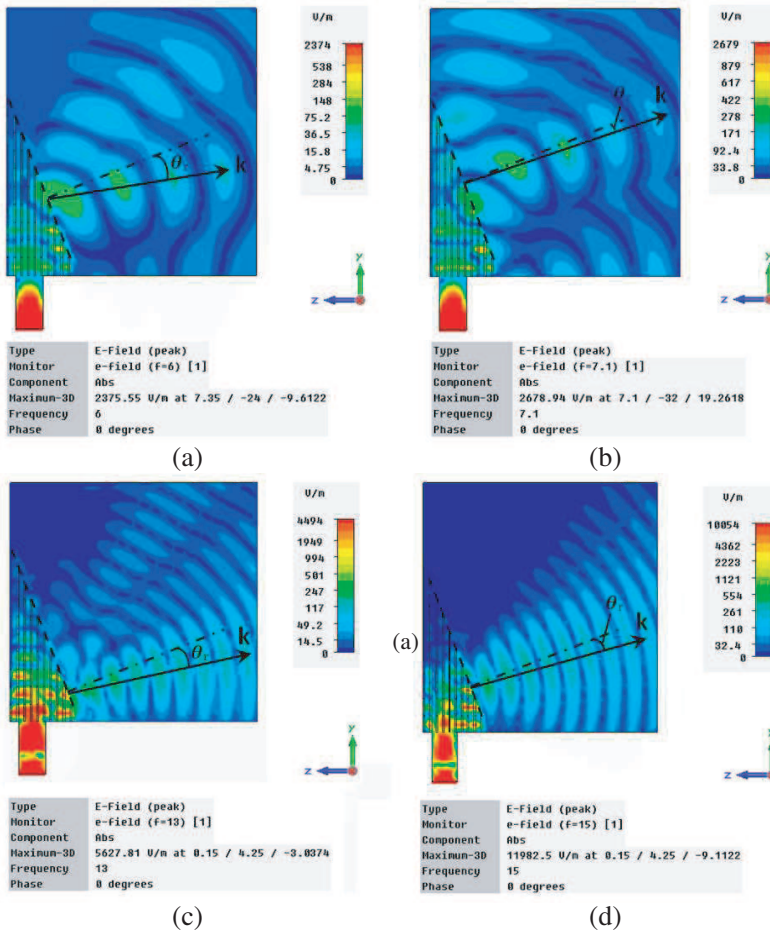


Figure 12. Prism-shaped structure simulation setup.



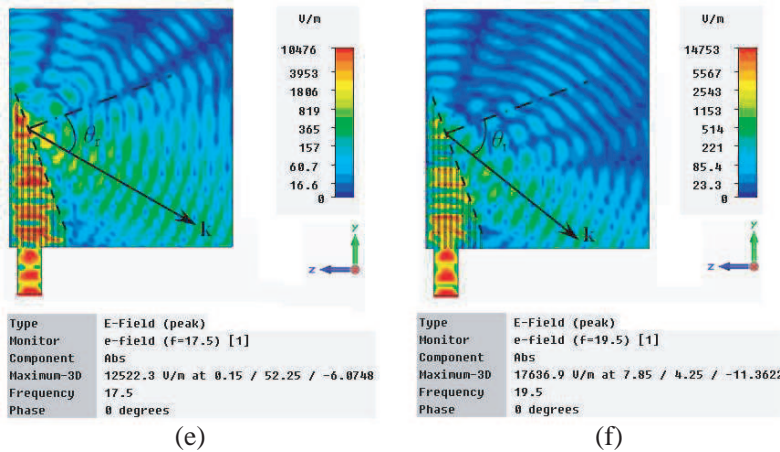


Figure 13. Electric field magnitude distribution for the refraction in a prism-shaped structure at the frequency of: (a) 6 GHz, (b) 7.1 GHz, (c) 13 GHz, (d) 15 GHz, (e) 17.5 GHz, and (f) 19.5 GHz.

7. CONCLUSION

This paper shares novel MTM design manipulating open stub-loaded SIR to produce tunable dual-band negative refractive index. Comprehensive analyses have been done throughout the letter concerning theoretical and simulation validation as well as the design techniques adopted. The simulation results show that the proposed structure exhibits two regions with negative real refractive index, n , values. In addition, based on these results the design proved to be efficient in producing materials with negative indices at lower fabrication costs on small-scale photolithographic printed circuit boards. The proposed MTM design is potentially applicable for improved quality microwave components like antennas and filters. It is flexible enough to be multifunctional, adaptive, and conformal besides having prospect for fulfilling the needs of next generation broadband communication technology.

ACKNOWLEDGMENT

The authors wish to thank the Universiti Putra Malaysia for providing us the research fund (RUGS Project No: 05-01-09-0722RU) to conduct this project.

REFERENCES

1. Veselago, V. G., "The electrodynamics of substances with simultaneously negative values of ϵ and μ ," *Sov. Phys. Usp.*, Vol. 10, 509–514, 1968.
2. Pendry, J. B., A. J. Holden, W. J. Stewart, and I. Youngs, "Extremely low frequency plasmons in metallic mesostructures," *Physical Review Letters*, Vol. 76, 4773–4776, 1996.
3. Pendry, J. B., A. J. Holden, D. J. Robbins, and W. J. Stewart, "Magnetism from conductors and enhanced nonlinear phenomena," *IEEE Transactions on Microwave Theory and Techniques*, Vol. 47, 2075–2084, 1999.
4. Smith, D. R., W. J. Padilla, D. C. Vier, S. C. Nemat-Nasser, and S. Schultz, "Composite medium with simultaneously negative permeability and permittivity," *Applied Physics Letters*, Vol. 84, 4184–4187, 2000.
5. Shelby, R., D. Smith, and S. Schultz, "Experimental verification of a negative index of refraction," *Science*, Vol. 292, 77–79, 2001.
6. Huangfu, J., L. Ran, H. Chen, X. Zhang, K. Chen, T. M. Grzegorzczak, and J. A. Kong, "Experimental confirmation of negative refractive index of a metamaterial composed of Ω -like metallic patterns," *Applied Physics Letters*, Vol. 84, 1537–1539, 2004.
7. Baena, J. D., R. Marques, and F. Medina, "Artificial magnetic metamaterial design by using spiral resonators," *Physical Review B*, Vol. 69, 014402/1–014402/5, 2004.
8. Zhou, J., T. Koschny, L. Zhang, G. Tuttle, and C. M. Soukoulis, "Experimental demonstration of negative index of refraction," *Applied Physics Letters*, Vol. 88, 221103/1–221103/3, 2006.
9. Kafesaki, M., I. Tsiapa, N. Katsarakis, Th. Koschny, C. M. Soukoulis, and E. N. Economou, "Left-handed metamaterial: The fishnet structure and its variations," *Physical Review B*, Vol. 75, 235114/1–235114/9, 2007.
10. Alici, K. B. and E. Ozbay, "A planar metamaterial: Polarization independent fishnet structure," *Photonics and Nanostructures-Fundamentals and Applications*, Vol. 6, No. 1, 102–107, 2008.
11. Isik, O. and K. P. Esselle, "Analysis of spiral metamaterials by use of group theory," *Metamaterials*, Vol. 3, No. 1, 33–43, 2009.
12. Wang, J., S. Qu, Z. Xu, J. Zhang, H. Ma, Y. Yang, and C. Gu, "Broadband planar left-handed metamaterials using split-ring resonator pairs," *Photonics and Nanostructures-Fundamentals and Applications*, Vol. 7, No. 2, 108–113, 2009.

13. Donzelli, G., A. Vallecchi, F. Capolino, and A. Schuchinsky, "Metamaterial made of paired planar conductors: Particle resonances, phenomena and properties," *Metamaterials*, Vol. 3, No. 1, 10–27, 2009.
14. Vallecchi, A., F. Capolino, A. G. Schuchinsky, and A. G. Schuchinsky, "2-D isotropic effective negative refractive index metamaterial in planar technology," *IEEE Microwave and Wireless Components Letters*, Vol. 19, No. 5, 269–271, 2009.
15. Wang, J., S. Qu, J. Zhang, H. Ma, Y. Yang, C. Gu, and X. Wu, "A tunable left-handed metamaterial based on modified broadside-coupled split-ring resonators," *Progress In Electromagnetics Research Letters*, Vol. 6, 35–45, 2009.
16. Ekmekci, E. and G. Turhan-Sayan, "Comparative investigation of resonance characteristics and electrical size of the double-sided SRR, BC-SRR and conventional SRR type metamaterials for varying substrate parameters," *Progress In Electromagnetics Research B*, Vol. 12, 35–62, 2009.
17. Zhou, X., Y. Liu, and X. Zhao, "Low losses left-handed materials with optimized electric and magnetic resonance," *Applied Physics A: Materials Science and Processing*, Vol. 98, No. 3, 643–649, 2009.
18. Zhu, C., J. -J. Ma, L. Chen, and C. -H. Liang, "Negative index metamaterials composed of triangular open-loop resonator and wire structures," *Microwave and Optical Technology Letters*, Vol. 51, No. 9, 2009.
19. Sabah, C., "Tunable metamaterial design composed of triangular split ring resonator and wire strip for S- and C- microwave bands," *Progress In Electromagnetics Research B*, Vol. 22, 341–357, 2010.
20. Nemer, S., B. Sauviac, B. Bayard, C. Nader, J. Bechara, and A. Khoury, "Modelling resonance frequencies of a multi-turn spiral for metamaterial applications," *Progress In Electromagnetics Research C*, Vol. 20, 31–42, 2011.
21. Alhawari, A. R. H., A. Ismail, M. A. Mahdi, and R. S. A. R. Abdullah, "Miniaturized ultra-wideband antenna using microstrip negative index metamaterial," *Electromagnetics*, Vol. 31, No. 6, 404–418, 2011.
22. Kwon, D.-H., D. H. Werner, A. V. Kildishev, and V. M. Shalaev, "Near-infrared metamaterials with dual-band negative-index characteristics" *Optics Express*, Vol. 15, No. 4, 1647–1652, 2007.
23. Hu, C. L., Liu, X. Chen, and X. Luo, "Expanding the band of negative permeability of a composite structure with dual-band negative permeability," *Optics Express*, Vol. 16, No. 26, 21544–

- 21549, 2008.
24. Hu, C., L. Liu, Z. Zhao, X. Chen, Q. Feng, and X. Luo, "Multimode magnetic responses in NIR and visible ranges," *Applied Physics B: Laser and Optics*, Vol. 96, No. 2–3, 439–443, 2009.
 25. Ekmekci, E. and G. Turhan-Sayan, "A novel dual-band metamaterial structure," *PIERS Proceedings*, 87–90, Moscow, Russia, August 18–21, 2009.
 26. Huang, C., Z. Zhao, Q. Feng, J. Cui, and X. Luo, "Metamaterial composed of wire pairs exhibiting dual band negative refraction," *Applied Physics B: Lasers and Optics*, Vol. 98, No. 2–3, 365–370, 2009.
 27. Gundogdu, T. F., K. Guven, M. Gokkavas, C. M. Soukoulis, and E. Ozbay, "A planar metamaterial with dual-band double-negative response at EHF," *IEEE Journal of Selected Topics in Quantum Electronics*, Vol. 16, No. 2, 376–379, 2010.
 28. Naghipourfar, M. and Z. Atlasbaf, "New dual-band DNG metamaterials," *Canadian Journal on Electrical and Electronics Engineering*, Vol. 2, No. 2, 47–56, February 2011.
 29. Chu, Q.-X. and F.-C. Chen, "A compact dual-band bandpass filter using meandering stepped impedance resonators," *IEEE Microwave and Wireless Components Letters*, Vol. 18, No. 5, 320–322, May 2008.
 30. Chu, Q.-X. and F.-C. Chen, "A novel dual-band bandpass filter using stepped impedance resonators with transmission zeros," *Microwave and Optical Technology Letters*, Vol. 50, No. 6, 1466–1468, June 2008.
 31. Velazquez-Ahumada, M. D. C., J. Martel, F. Medina, and F. Mesa, "Application of stub loaded folded stepped impedance resonators to dual band filter design," *Progress In Electromagnetics Research*, Vol. 102, 107–124, 2010.
 32. Namsang, A. and P. Akkaraekthalin, "Microstrip bandpass filters using end-coupled asymmetrical step-impedance resonators for wide-spurious response," *Progress In Electromagnetics Research C*, Vol. 14, 53–65, 2010.
 33. Xiao, J.-K. and H.-F. Huang, "New dual-band bandpass filter with compact sir structure," *Progress In Electromagnetics Research Letters*, Vol. 18, 125–134, 2010.
 34. Zhang, X. Y., C. H. Chan, Q. Xue, and B.-J. Hu, "Dual-band bandpass filter with controllable bandwidths using two coupling paths," *IEEE Microwave and Wireless Components*

- Letters*, Vol. 20, No. 11, 616–618, November 2010.
35. Makimoto, M. and S. Yamashita, *Microwave Resonators and Filters for Wireless Communication*, Springer-Verlag, Berlin, Heidelberg, 2001.
 36. Razalli, M. S., A. Ismail, M. A. Mahdi, and M. N. Bin Hamidon, “Novel compact microstrip ultra-wideband filter utilizing short-circuited stubs with less vias,” *Progress In Electromagnetics Research*, Vol. 88, 91–104, 2008.
 37. Chen, F.-C., Q.-X. Chu, and Z.-H. Tu, “Design of compact dual-band bandpass filter using short stub loaded resonator,” *Microwave and Optical Technology Letters*, Vol. 51, No. 4, 959–963, April 2009.
 38. Li, B., X. Wu, N. Yang, and W. Wu, “Dual-band equal/unequal Wilkinson power dividers based on coupled-line section with short-circuited stub,” *Progress In Electromagnetics Research*, Vol. 111, 163–178, 2011.
 39. Kuo, J. T. and C. Y. Tsai, “Periodic stepped-impedance ring resonator (PSIRR) bandpass filter with a miniaturized area and desirable upper stopband characteristics,” *IEEE Transactions on Microwave Theory and Techniques*, Vol. 54, No. 3, 1107–1112, March 2006.
 40. Chen, C. F., T. Y. Huang, and R. B. Wu, “Design of dual- and triple-passband filters using alternately cascaded multiband resonators,” *IEEE Transactions on Microwave Theory and Techniques*, Vol. 54, No. 9, 3550–3558, September 2006.
 41. Weng, M. H., H. W. Wu, and Y. K. Su, “Compact and low-loss dual-band bandpass filter using pseudo-interdigital stepped impedance resonators for WLANs,” *IEEE Microwave and Wireless Components Letters*, Vol. 17, No. 3, 187–189, March 2007.
 42. Chen, F.-C. and Q.-X. Chu, “Novel multistub loaded resonator and its application to high-order dual-band filters,” *IEEE Transactions on Microwave Theory and Techniques*, Vol. 58, No. 6, 1551–1556, June 2010.
 43. Computer Simulation Technology (CST) Microwave Studio, Version 2010.
 44. Hong, J.-S. and M. J. Lancaster, *Microstrip Filter for RF/Microwave Applications*, Wiley, New York, 2001.
 45. Smith, D. R., S. Shultz, P. Markos, and C. M. Soukoulis, “Determination of effective permittivity and permeability of metamaterials from reflection and transmission coefficients,”

- Physics Review B*, Vol. 65, 195104-195101–95104-195105, 2002.
46. Chen, X., T. M. Grzegorzcyk, B.-I. Wu, J. Pacheco, and J. A. Kong, “Robust method to retrieve the constitutive effective parameters of metamaterials,” *Physical Review E* 70, 016608/1–016608/7, 2004.
 47. Smith, D. R., D. C. Vier, T. Koschny, and C. M. Soukoulis, “Electromagnetic parameter retrieval from inhomogeneous metamaterials,” *Physical Review E*, Vol. 71, 036617/1–036617/11, 2005.
 48. Grzegorzcyk, T. M., M. Nikku, X. Chen, B.-I. Wu, and J. A. Kong, “Refraction laws for anisotropic media and their application to left-handed metamaterials,” *IEEE Transactions on Microwave Theory and Techniques*, Vol. 53, No. 4, 1443–1450, 2005.
 49. Wu, Q., P. Pan, F.-Y. Meng, L.-W. Li, and J. Wu, “A novel flat lens horn antenna designed based on zero refraction principle of metamaterials,” *Applied Physics A*, Vol. 87, 151–156, 2007.